Molecular Dynamics Simulations of pH-Dependent Ciprofloxacin Adsorption to Na-montmorillonite

Rogers E. Swai and Michael Holmboe‡

(*Umeå University, Chemistry Department, Umeå, Sweden*)
‡*Correspondence: michael.holmboe@umu.se*

Supporting Information

Table of Contents

1. CIP molecular structure

1.1 CIP dimensions

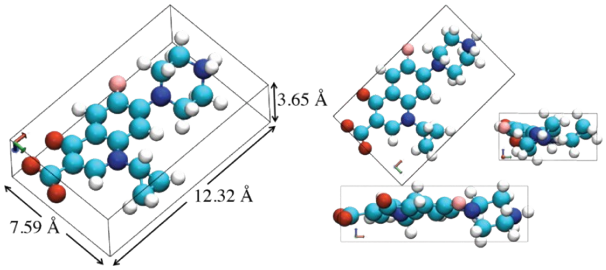

Fig. S1 CIP structure after DFT geometry optimization. Red=O, blue=N, white=H, Cyan=C, and Pink=F.

1.2 Reference structure conformations for RMSD

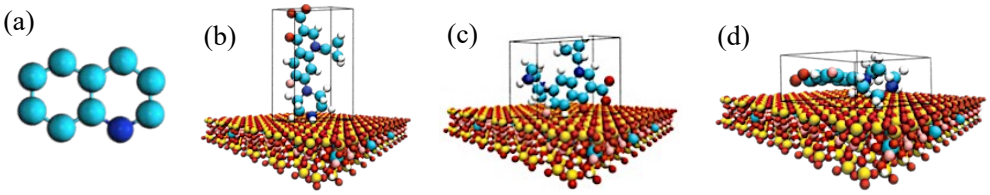

Fig. S2 Selected reference structures for RMSD fitting: Cross (b), Side (c), and Flat (d). RMSD was done by fitting to the aromatic core (a) after removing rotational and translation motions along the *xy*-plane.

1.3 Gaff atom types assignment

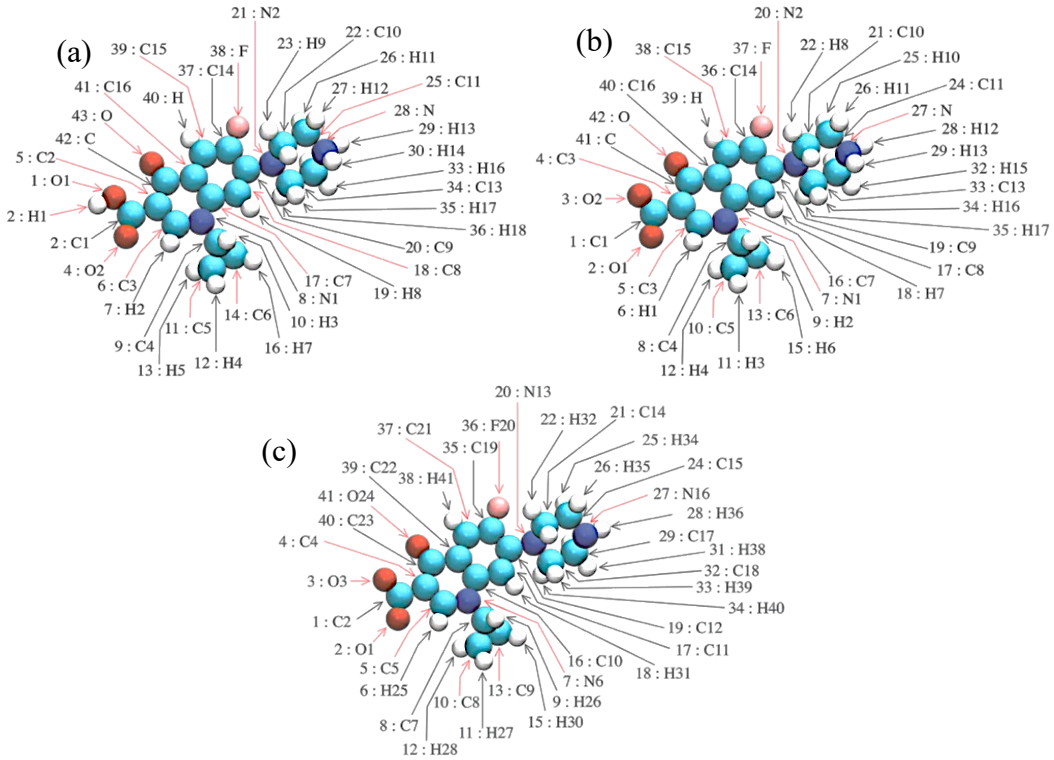

Fig. S3 Atom type indexing. CIP^{+} (a), $CIP^{+/-}$ (b), CIP^{-} (c). Refer to Table S1 for each atom's charges.

2. System setup

2.1 Open and closed systems

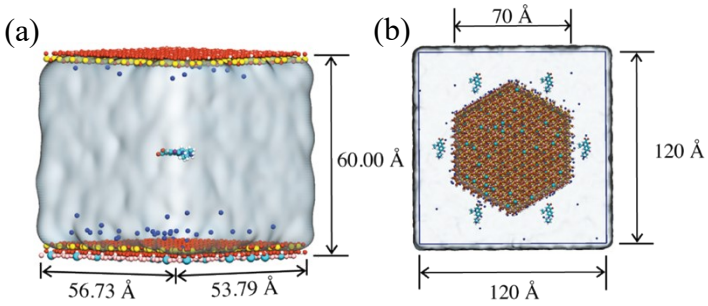

Fig. S4 Na-MMT-CIP closed system to study CIP bulk-surface migration (a) and open system to study CIP bulk-interlayer migration (intercalation), a view from the top (b).

2.2 Biased umbrella sampling simulations

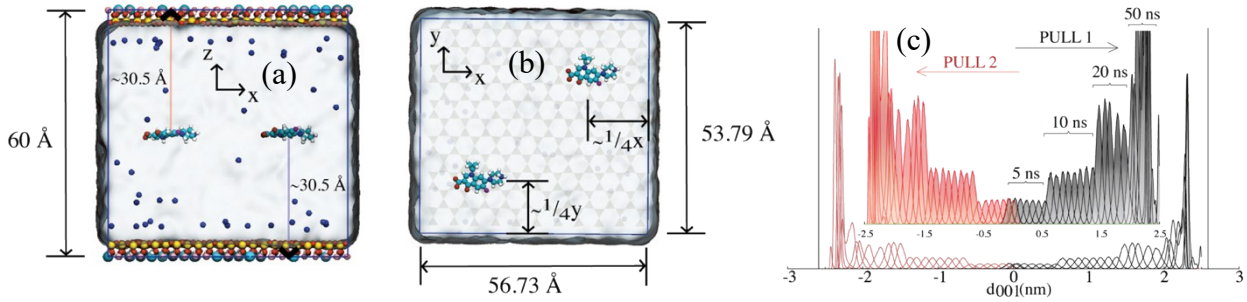

Fig. S5 Placement of CIP molecule for the US simulations. Side view (a), top view (b), tethering umbrella windows and selected simulation times (c)

2.3 Free energy of perturbation (FEP) simulations

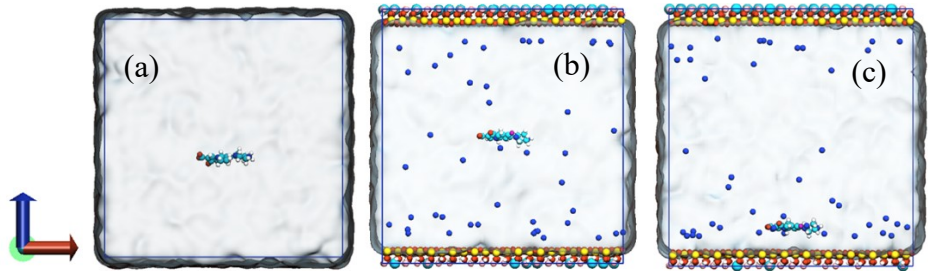

Fig. S6 The three selected regions for CIP free energy of perturbation (FEP) simulations. Water box (a), Middle of MMT, mesopore (b), and at the surface of MMT, adsorbed (c).

3. Complementary results

3.1 Interlayer species distribution

3.1.1 Density profiles.

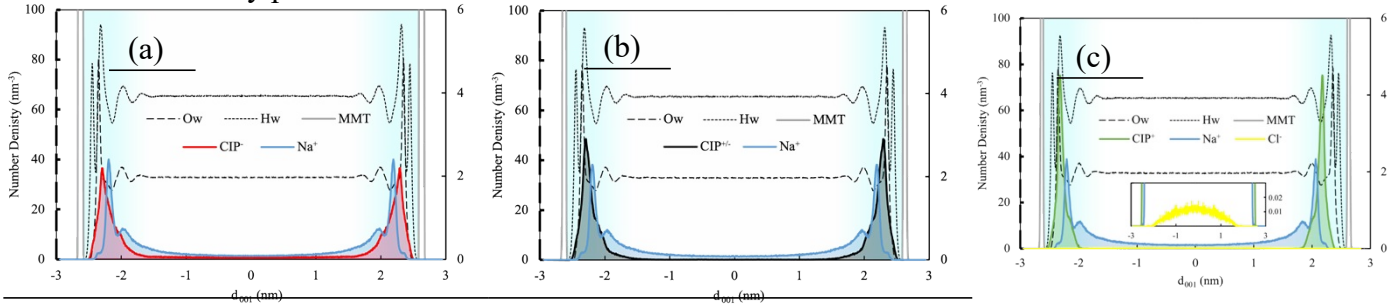

Fig. S7 CIP species density profiles normal to the MMT surface. Use the dashed axis (left) for dashed curves.

3.1.2 Functional group distribution

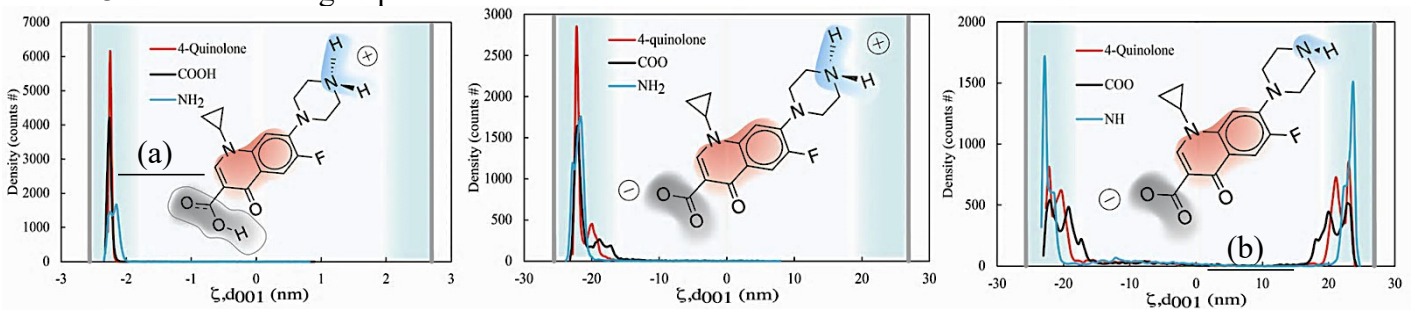

Fig S8 Unnormalized density distributions of CIP functional groups. CIP^{+} (a), $CIP^{+/-}$ (b), and CIP^{-} (c).

3.2 CIP interaction modes

3.2.1 CIP-MMT adsorption modes when intercalating open system

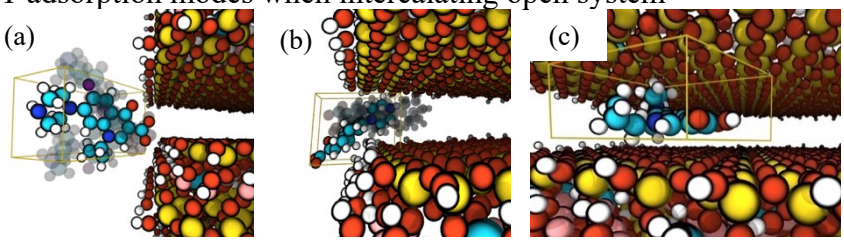

Fig. S9 CIP^{-} carboxylate/ketone interaction with the edge protons (a). $CIP^{+/-}$ both edge and surface interactions (b) multiple snapshots were overlain. CIP^{+} basal surface interaction (c)

3.2.2 CIP-MMT configurations from dominant clusters

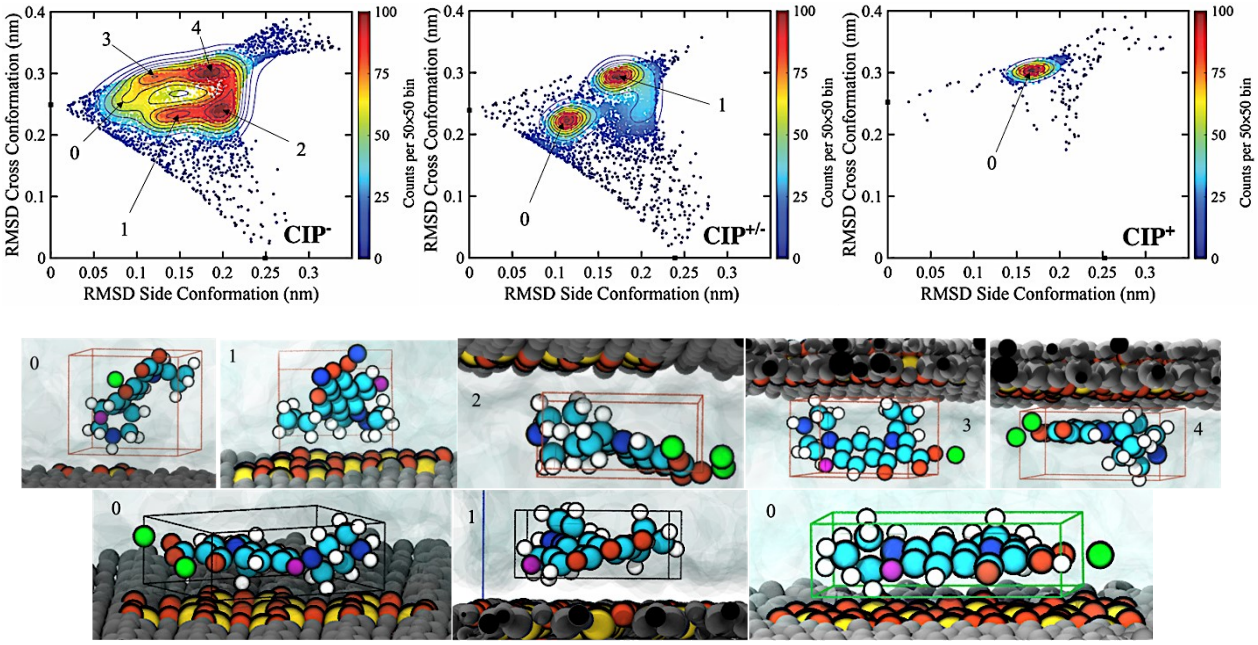

Fig. 10 Top row, selected CIP cluster populations. Middle row, CIP^{-} representative configurations from the dominant populations, dimension boundaries are marked in red. Bottom row, $CIP^{+/-}$ and CIP^{+} boundaries are marked with black and green rectangles, respectively. Green ball = Na^{+} within 3 Å of CIP O-atoms (red balls on the molecule). MMT surface atoms within 5 Å of the CIP molecule are in color (Si = yellow, O = oxygen), while the rest are all displayed in a shade of gray.

3.3 Heat maps

3.3.1 CIP bulk-interlayer exchange behaviour

3.3.1.1 One CIP.

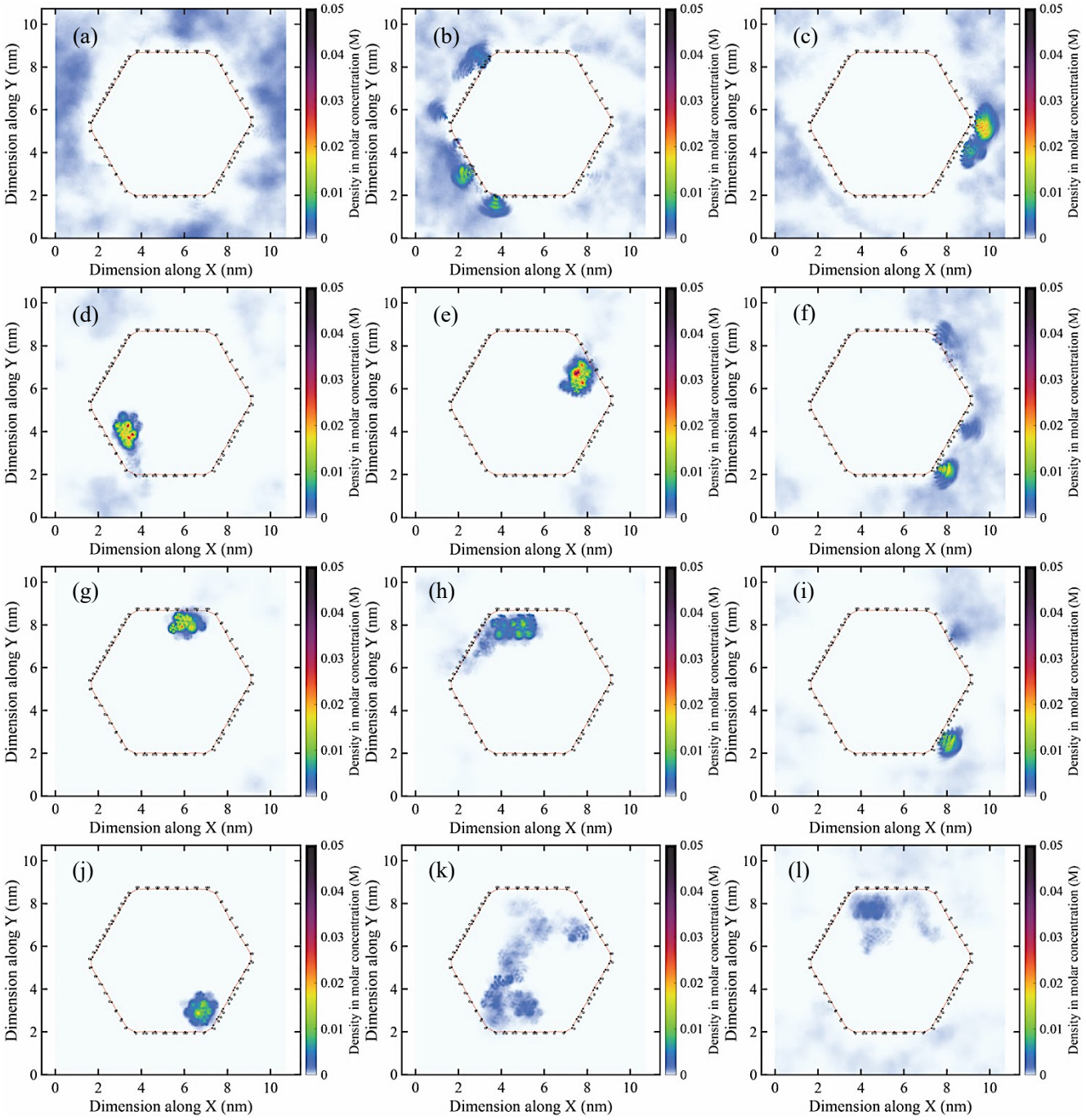

Fig. S11 Intercalation of 1 CIP molecule at varying water content Top–Bottom 1W, 2W, 3W, and 4W, CIP^{+}, $CIP^{+/-}$, CIP^{-} (left, center, and right, respectively).

3.3.1.2 Three CIP.

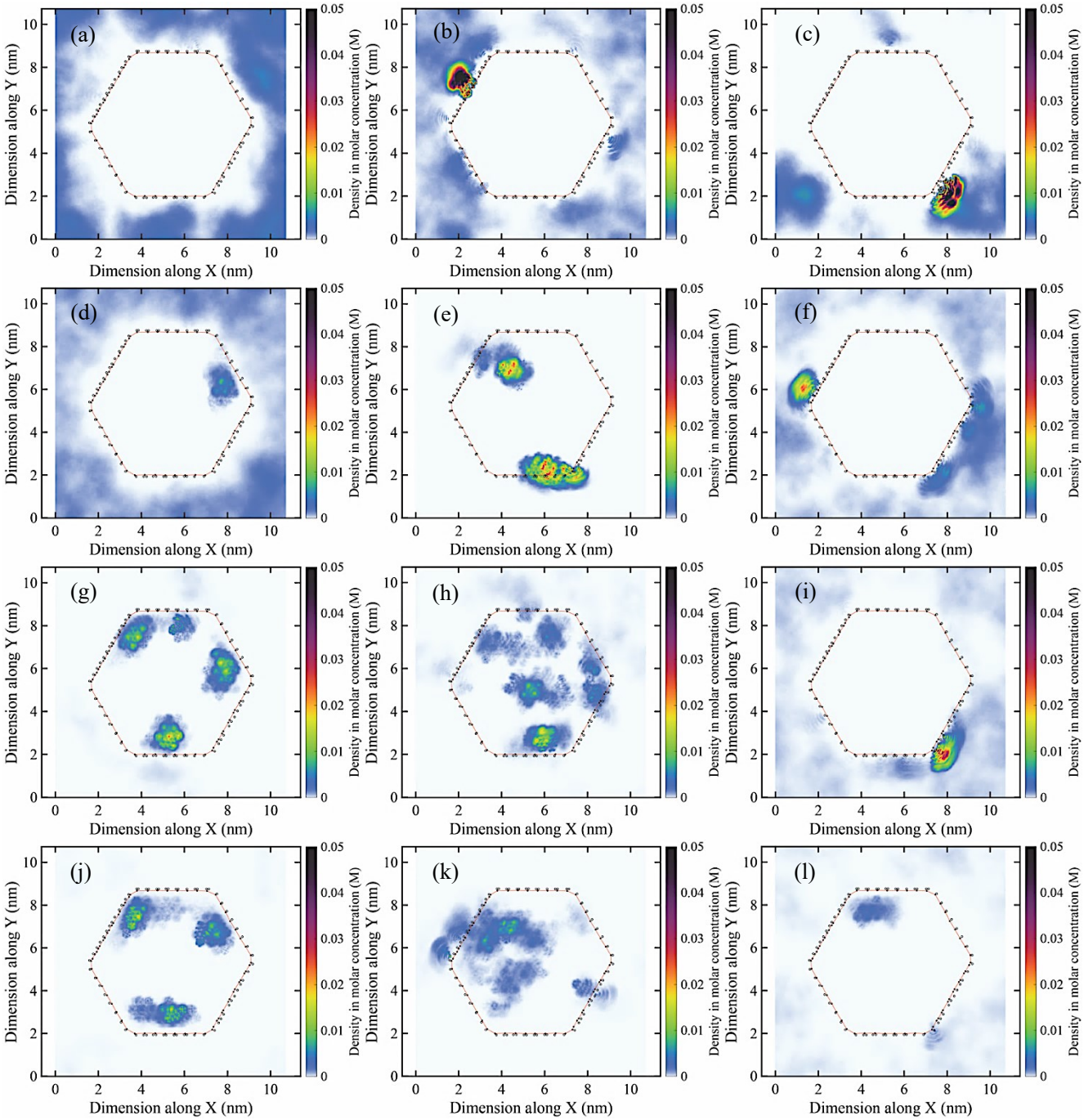

Fig. S12 Intercalation of 3 CIP molecules at varying water content Top–Bottom 1W, 2W, 3W, and 4W, CIP^{+}, $CIP^{+/-}$, CIP^{-} (left, center, and right, respectively).

3.3.2 CIP interlayer-bulk exchange behaviour

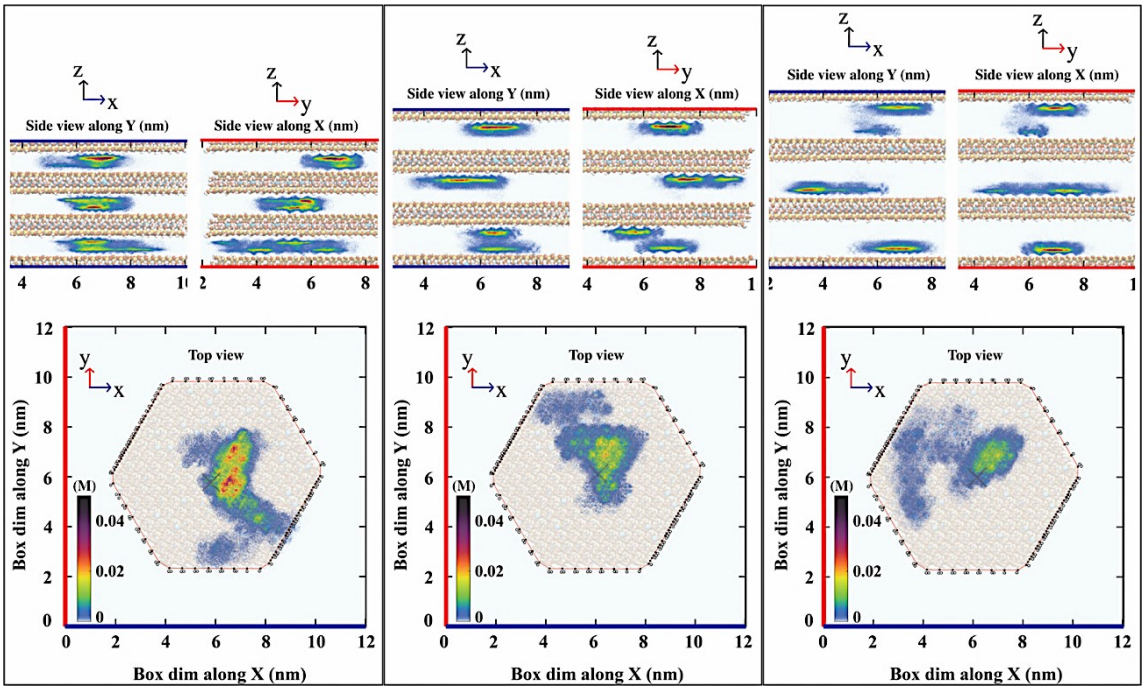

Fig. S13 Investigation of CIP^{+} interlayer egress at varying water content. Top–Bottom 2W, 3W, and 4W. Heat maps shows CIP^{+} remains in the interlayer over the course of the simulation.

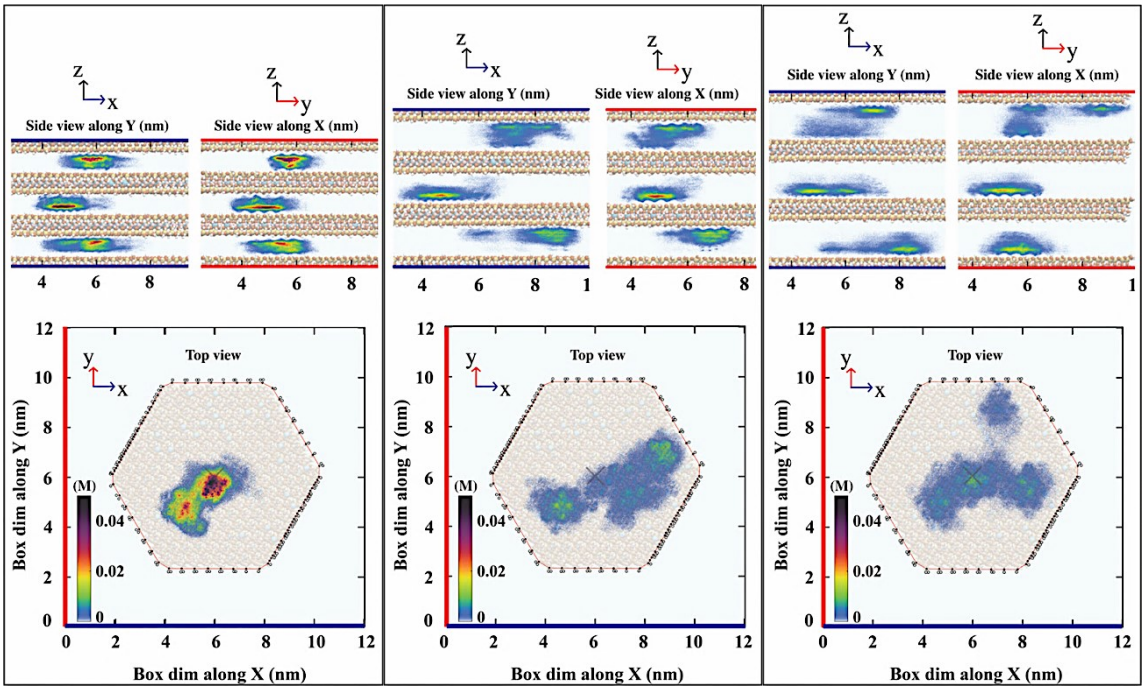

Fig. S14 Investigation of $CIP^{+/-}$ interlayer egress at varying water content Top–Bottom 2W, 3W, and 4W. Heat maps shows $CIP^{+/-}$ remains in the interlayer over the course of the simulation.

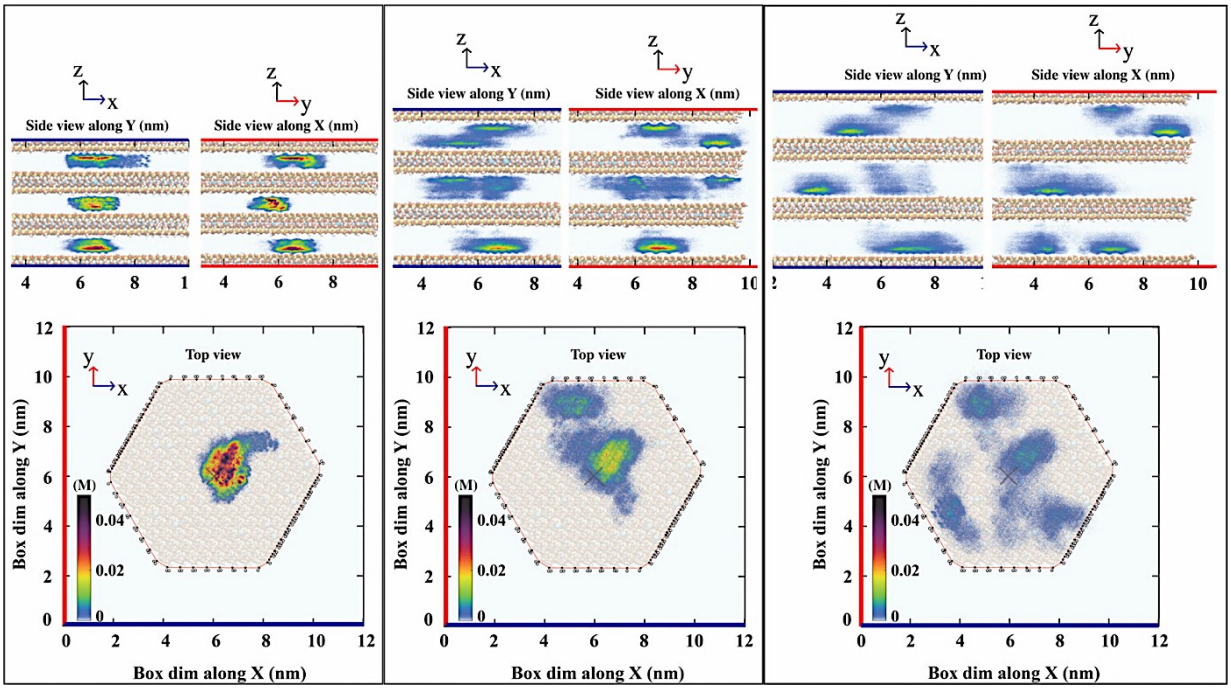

Fig. S15 Investigation of CIP^- interlayer egress at varying water content Top–Bottom 2W, 3W, and 4W. Heat maps shows CIP^- remains in the interlayer over the course of the simulation.

3.4 Cluster analysis from RMSD fitting projections

3.4.1 Analysis of CIP^- dominant cluster configurations

1) Selected cluster

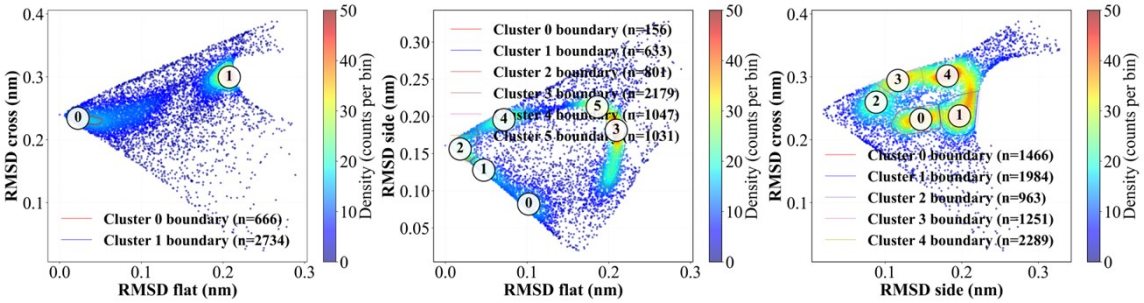

Fig. S16 Cluster selections for the flat versus cross (left), flat versus side (middle), and side versus cross (right)

2) CIP^- functional groups Na^+ coordination environments

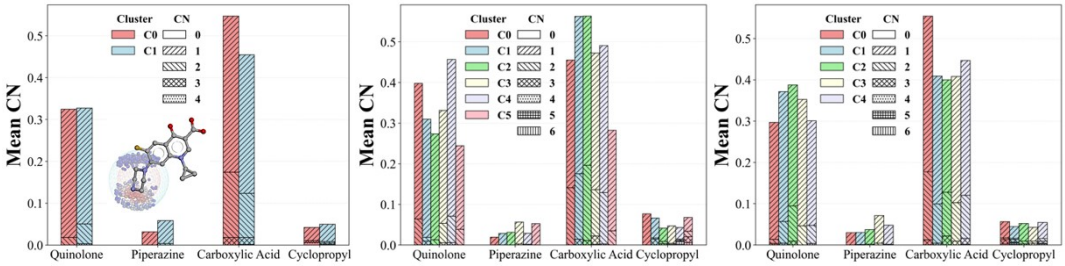

Fig. S17 Na^+–CIP^-(functional group) coordination for the flat versus cross (left), flat versus side (middle), and side versus cross (right) projections. Analysis performed up to within the first peak of the Na^+–functional group RDFs

3) CIP^- functional groups MMT surface interaction

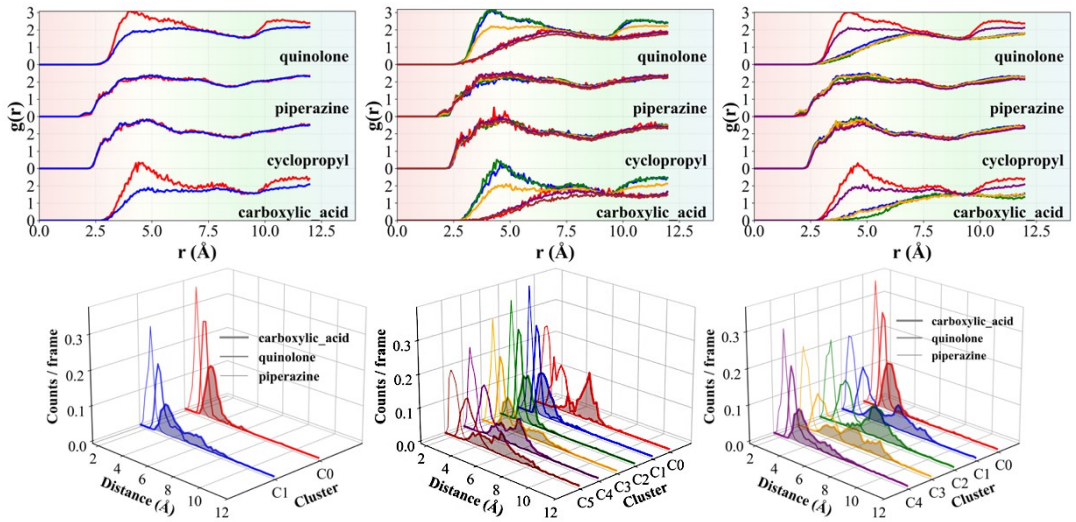

Fig. S18 CIP⁻(functional groups)–MMT (basal oxygen) RDFs (Top) and spatial distribution across z-dimension (bottom) for the flat versus cross (left), flat versus side (middle), and side versus cross projections (right). Cluster 0 = red, cluster 1 = blue, cluster 2 = green, cluster 3 = orange, cluster 4 = purple, cluster 5 = brown.

4) CIP⁻ functional groups Na^+ mediated surface adsorption

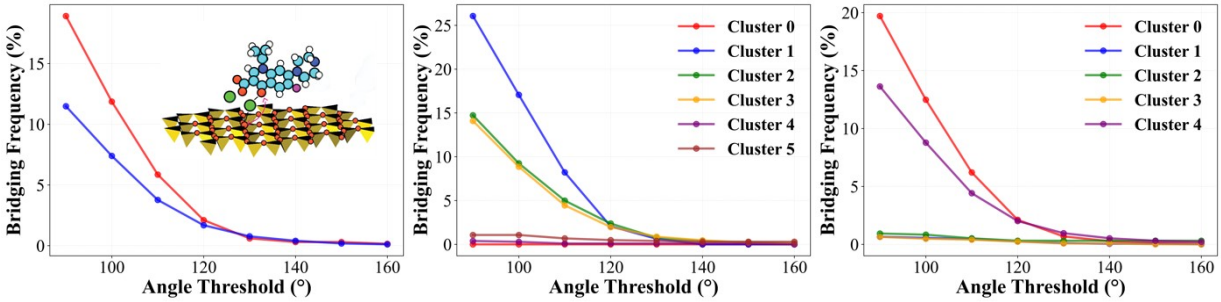

Fig. S19 ∠CIP⁻(carboxylate oxygen)-Na^+-MMT interaction mode analysis. For the flat versus cross (left), flat versus side (middle), and side versus cross (right) projections. Angle 140 °-160° moderate bridge, 160°-180° optimal bridge effect, and angle 90°-140° sub-optimal screening effect.

3.4.2 Analysis of CIP$^{+/-}$ dominant cluster configurations

1) Selected configuration clusters

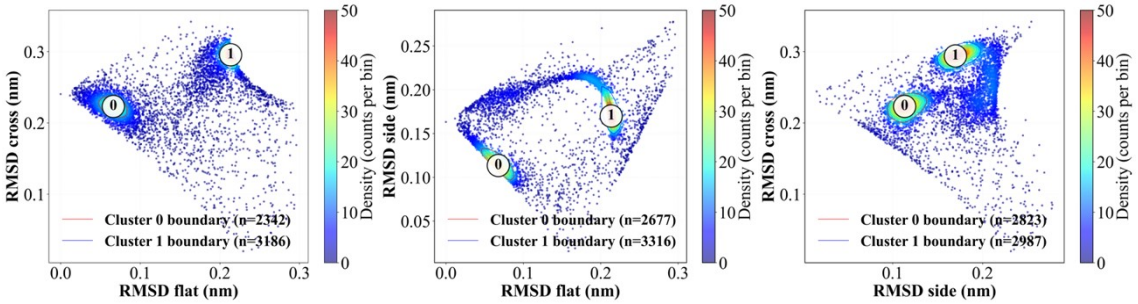

Fig. S20 Cluster selections for the flat versus cross (a), flat versus side (b), and side versus cross projections (c)

2) CIP$^{+/-}$ functional groups Na^+ coordination environments

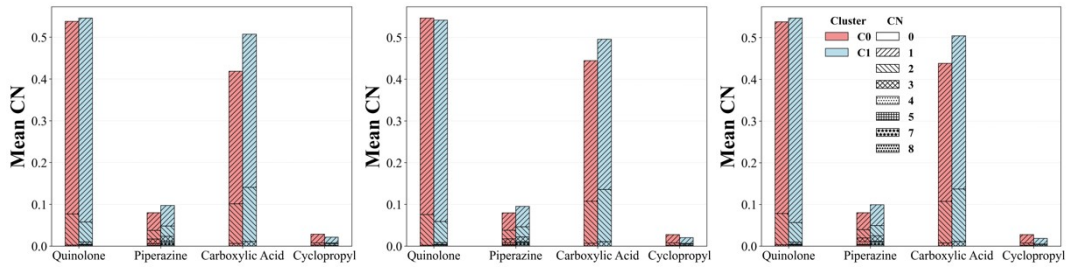

Fig. S21 Na^+–$CIP^{+/-}$(functional group) coordination for the flat versus cross (left), flat versus side (middle), and side versus cross (right) projections. Analysis performed up to within the first peak of the Na^+–functional group RDFs

3) $CIP^{+/-}$ functional groups MMT surface interaction

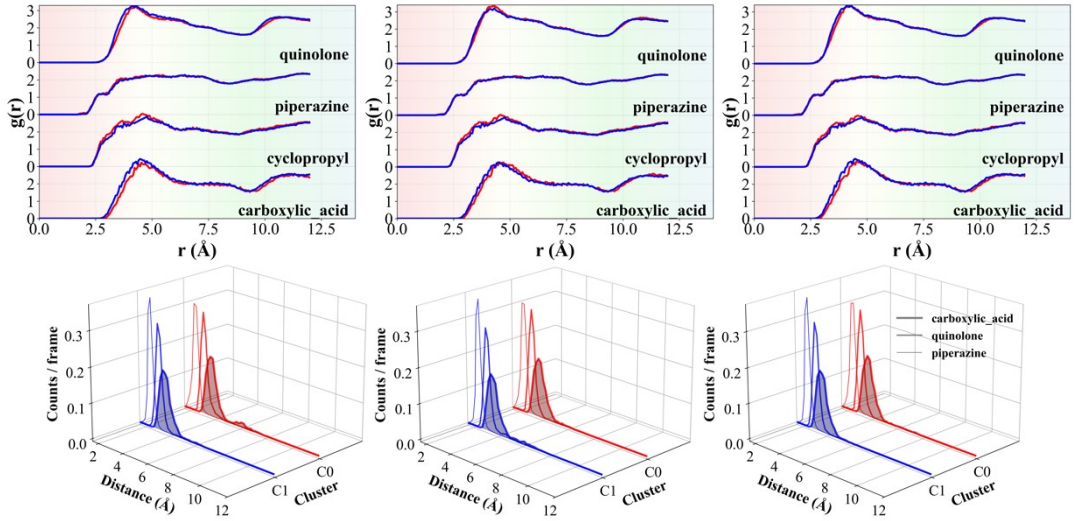

Fig. S22 $CIP^{+/-}$(functional groups)–MMT (basal oxygen) RDFs and spatial distribution across z-dimension (bottom) for the flat versus cross (a), flat versus side (b), and side versus cross projections (c)

4) $CIP^{+/-}$ functional groups Na^+ mediated surface adsorption

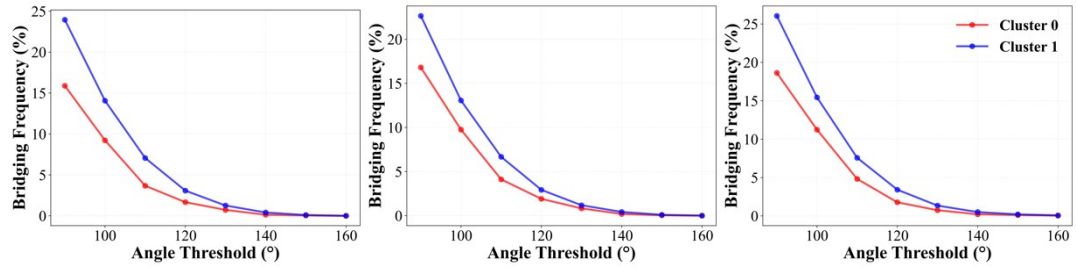

Fig. S23 ∠$CIP^{+/-}$-Na^+-MMT interaction mode analysis. For the flat versus cross (left), flat versus side (middle), and side versus cross (right) projections. Angle 140 °-160° moderate bridge, 160°-180° optimal bridge effect, and angle 90°-140° sub-optimal screening effect

3.4.3 Analysis of CIP^+ dominant cluster configurations

1) Selected configuration clusters

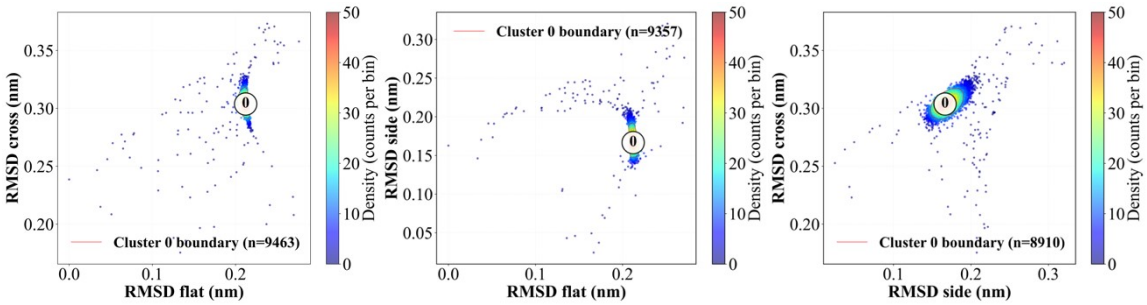

Fig. S24 Cluster selections for the flat versus cross (a), flat versus side (b), and side versus cross projections (c)

2) CIP^+ functional groups Na^+ coordination environments

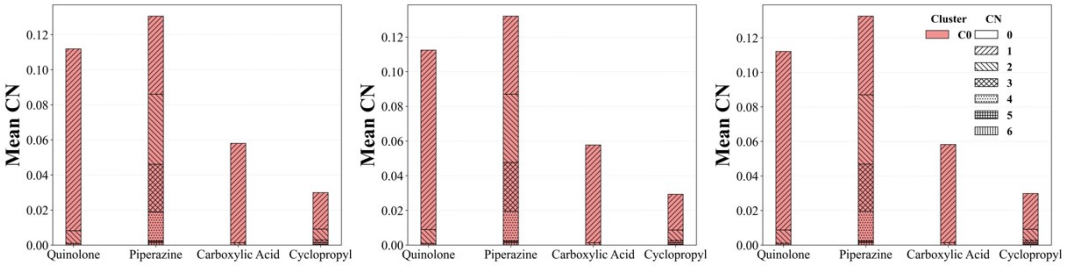

Fig. S25 Na^+–CIP^+(functional group) coordination for the flat versus cross (a), flat versus side (b), and side versus cross projections (c). Analysis performed up to withinto the first peak of the Na^+–functional group RDFs

3) CIP^+ functional groups MMT surface interaction

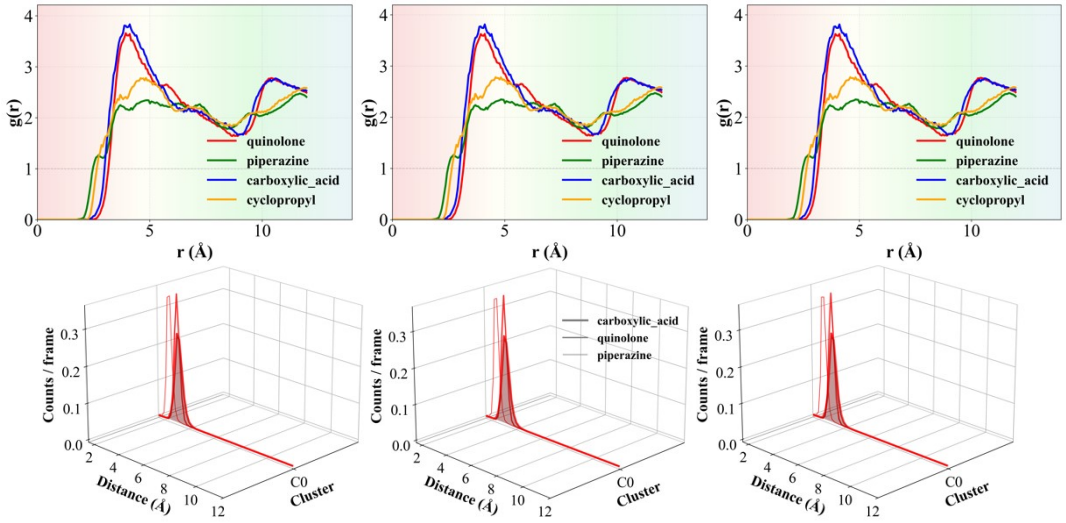

Fig. S26 CIP^+(functional groups)–MMT (basal oxygen) RDFs (Top) and spatial distribution across z-dimension (bottom) for the flat versus cross (a), flat versus side (b), and side versus cross projections (c)

4) CIP^+ functional groups Na^+ mediated surface adsorption

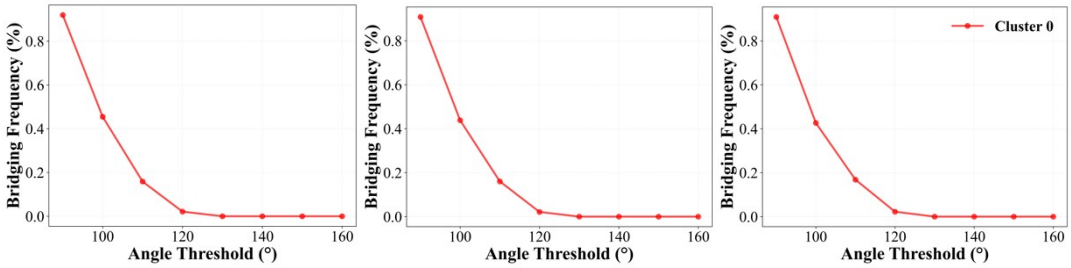

Fig. S27 ∠CIP$^{+/-}$-Na^{+}-MMT interaction mode analysis. For the flat versus cross (left), flat versus side (middle), and side versus cross (right) projections. Angle 140 °-160° moderate bridge, 160°-180° optimal bridge effect, and angle 90°-140° sub-optimal screening effect

4 PMF profile

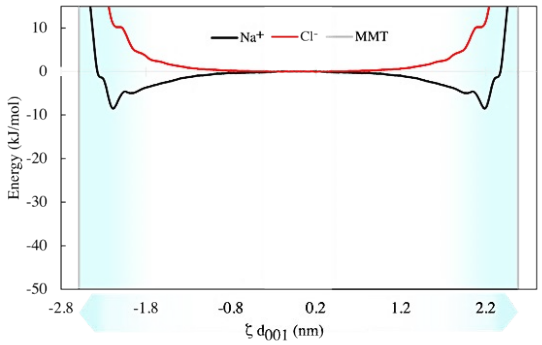

Fig. S28 Potential of mean force (PMF) landscapes for the interlayer Na^{+} and the charge-balancing Cl^{-}.

5 Electrostatic surface potential (ESP)

Quantum wave function calculations for the electrostatic surface potential (ESP) of the CIP molecules were performed in the Multiwfn program[3].

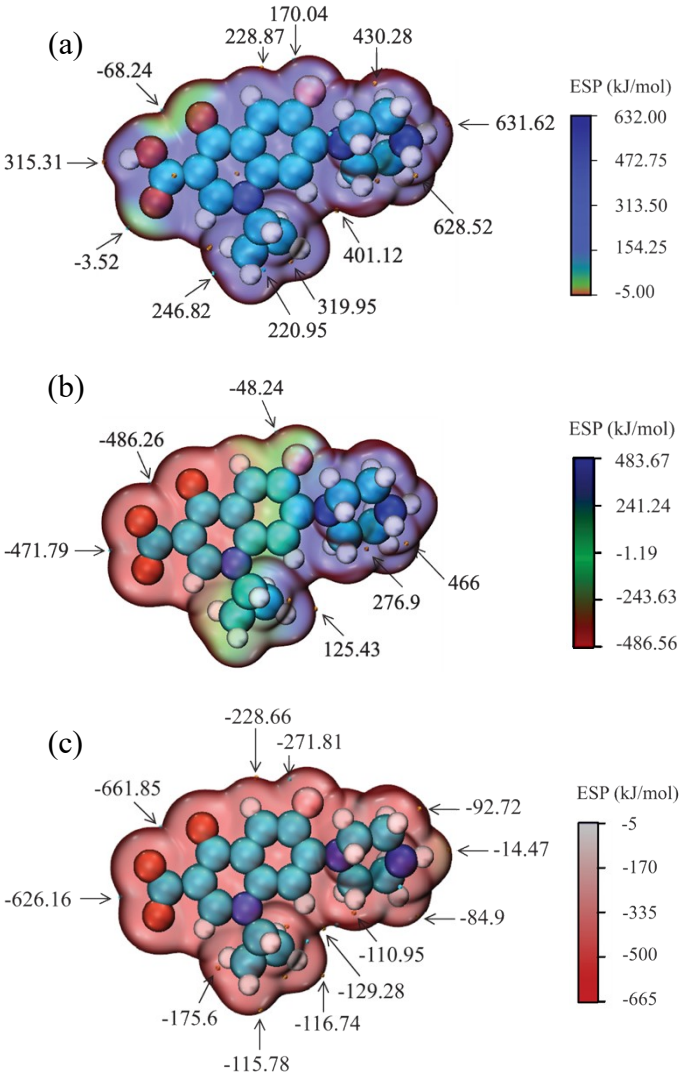

Fig. S29 Electrostatic surface potential (ESP) for CIP^+ (a), $CIP^{+/-}$ (b), and CIP^- (c) (Energy in kJ/mol).

References

1. Holmboe M. ATOM: A Matlab Package for Manipulation of Molecular Systems. Clays Clay Miner. 2019;67(5):419–26.
2. WilliamHumphrey, AndrewDalke, KlausSchulten. VMD: Visual molecular dynamics. J Mol Graph. 1996;14(1):33–8.
3. Lu T, Chen F. Multiwfn: A multifunctional wavefunction analyzer. J Comput Chem. 2012;33(5):580–92.

Appendices

Table S1. CIP Gaff atom-types and RESP A1 charges

CIP^-			$CIP^{+/-}$			CIP^+		
Type	Atom	Charge	Type	Atom	Charge	Type	Atom	Charge
c	C2	0.9328	c	C1	0.9368	oh	O1	-0.587
o	O1	-0.8168	o	O1	-0.7978	ho	H1	0.457
o	O3	-0.8168	o	O2	-0.7978	c	C1	0.6909
cc	C4	-0.2432	cc	C2	-0.2312	o	O2	-0.5885
cd	C5	-0.016	cd	C3	-0.028	cc	C2	-0.1384
h4	H25	0.17	h4	H1	0.183	cd	C3	-0.1086
na	N6	-0.3492	na	N1	-0.3382	h4	H2	0.1727
cx	C7	0.1675	cx	C4	0.1525	na	N1	0.0716
h1	H26	0.0767	h1	H2	0.0747	cx	C4	0.0757
cx	C8	-0.1379	cx	C5	-0.1319	h1	H3	0.0871
hc	H27	0.07795	hc	H3	0.08145	cx	C5	-0.2703
hc	H28	0.07795	hc	H4	0.08145	hc	H4	0.1439
cx	C9	-0.1379	cx	C6	-0.1319	hc	H5	0.1439
hc	H29	0.07795	hc	H5	0.08145	cx	C6	-0.2703
hc	H30	0.07795	hc	H6	0.08145	hc	H6	0.1439
ca	C10	0.132	ca	C7	0.141	hc	H7	0.1439
ca	C11	-0.24	ca	C8	-0.238	ca	C7	-0.0362
ha	H31	0.134	ha	H7	0.127	ca	C8	-0.1158
ca	C12	0.1346	ca	C9	0.0886	ha	H8	0.0639
nh	N13	-0.63	nh	N2	-0.636	ca	C9	0.022
c3	C14	0.1833	c3	C10	0.1643	nh	N2	-0.1803
h1	H32	0.0462	h1	H8	0.08345	c3	C10	0.076
h1	H33	0.0462	h1	H9	0.08345	h1	H9	0.0662
c3	C15	0.1588	c3	C11	0.0993	h1	H10	0.0662
h1	H34	0.03145	hx	H10	0.1087	c3	C11	-0.1545
h1	H35	0.03145	hx	H11	0.1087	hx	H11	0.1495
n3	N16	-0.8202	n4	N	-0.762	hx	H12	0.1495
hn	H36	0.3548	hn	H12	0.4443	n4	N	-0.1608
c3	C17	0.1588	hn	H13	0.4443	hn	H13	0.2955
h1	H37	0.03145	c3	C12	0.0993	hn	H14	0.2955
h1	H38	0.03145	hx	H14	0.1087	c3	C12	-0.1545
c3	C18	0.1833	hx	H15	0.1087	hx	H15	0.1495
h1	H39	0.0462	c3	C13	0.1643	hx	H16	0.1495
h1	H40	0.0462	h1	H16	0.08345	c3	C13	0.076
ca	C19	0.0329	h1	H17	0.08345	h1	H17	0.0662
f	F20	-0.1549	ca	C14	0.0399	h1	H18	0.0662
ca	C21	-0.068	f	F	-0.1549	ca	C14	0.1221
ha	H41	0.169	ca	C15	-0.056	f	F	-0.1717
ca	C22	-0.19	ha	H	0.185	ca	C15	-0.0995
c	C23	0.5601	ca	C16	-0.17	ha	H	0.1837
o	O24	-0.5501	c	C	0.5561	ca	C16	-0.0638
			o	O	-0.5211	c	C	0.4782
						o	O	-0.5061

Table S2. Quantum calculation results for different ESP-related properties

Property	CIP^+	$CIP^{+/-}$	CIP^-
The volume enclosed by the isosurface ($Å^3$)	372.54	372.67	376.01
Minimum value of the surface potentials (kJ/mol)	-68.24	-514.14	-688.76
Maximum values of the surface potentials (kJ/mol)	631.62	490.49	-17.20
Positive average potential (kJ/mol)	290.95	210.02	0.0
Negative average potential (kJ/mol)	-28.52	-204.04	-271.30
Overall average potential (kJ/mol)	274.89	1.30	-271.30
Overall surface area ($Å^2$)	333.61	336.91	338.75
Positive surface area ($Å^2$)	316.85	167.08	0.0
Negative surface area ($Å^2$)	16.76	169.83	338.75
Molecular polarity index (MPI) (kJ/mol)	277.76	207.00	-271.30
Nonpolar surface area (|ESP| <= 10 kcal/mol) ($Å^2$)	25.48	50.85	2.54
Polar surface area (|ESP| > 10 kcal/mol) ($Å^2$)	308.13	286.06	336.21